

Unifying uncertainties for rotor-like quantum systems

Ladislav Mišta, Jr.,^{1,*} Matouš Mišta,^{2,†} and Zdeněk Hradil^{1,‡}

¹*Department of Optics, Palacký University, 17. listopadu 12, 771 46 Olomouc, Czech Republic*

²*Gymnázium Olomouc-Hejčín, Tomkova 45, 779 00 Olomouc, Czech Republic*

Quantum rotor represents the second simplest model after the harmonic oscillator with profound interdisciplinary but yet unexplored implications. It overreaches its mechanical meaning with significant consequences and promising applications in, e.g., singular optics, super-conductive circuits with Josephson junction or optimal pulse shaping in time frequency domains at ultimate quantum limit. Quantification of complementarity between angular momentum and angular variable is essential for exploitation of this canonical pair in quantum metrology. Whereas the natural measures for position and momentum are variances, the uncertainty associated with angular variable can be linked to moments of inertia of the unit ring about axes passing through its center of mass. This interpretation provides variants for saturable uncertainty relations which can be further used in quantum metrology of the quantum rotor and explains ambiguities in choice of possible uncertainty measures associated with sine and cosine functions of angular variable. Special attention will be paid to uncertainty products which are exactly or approximately minimised by von Mises states, which play the role of squeezed states for quantum rotor and allow optimal detection of quantum states at the ultimate limits.

I. INTRODUCTION

Quantum mechanics imposes rules, which are establishing sophisticated network of interconnected and subtle conditions, which are distinguishing the realm of quantum effects from the classical world, and impose ultimate bounds on the precision of involved variables. This is, for instance, the case of the celebrated Heisenberg uncertainty relation for the canonical pair of position and momentum of a (quantum) particle. The uncertainty relation states that, loosely speaking, the momentum and position of a particle cannot be measured precisely at the same time. Interestingly, this concept generalizes to other pairs of canonical observables, for instance the quadrature operators of the electromagnetic field. In this case, the real part of the field can take the role of canonical position, whereas the imaginary part can be considered as the canonical momentum. These and similar examples have laid the foundations of quantum optics and quantum information processing. The important milestones on this route built systematically over one century were uncertainty relations, coherent (squeezed) states, Einstein-Podolsky-Rosen (EPR) states [1], Arthurs-Kelly concept of simultaneous detection of non-commuting variables [2, 3], concept of Bell-like measurement and representation of quantum state in phase-space pioneered by Wigner [4], Husimi [5] or Glauber [6]. On the top of those fundamental concepts there are several valuable protocols allowing process quantum information such as quantum teleportation [7] or quantum cryptography [8]. These examples can be cast into the same formal framework since they obey the commutation rule of the Lie algebra of the Heisenberg group, $[x, p] = i\hbar$, and observables are related by continuous Fourier transformation. Similar structure is associated with conservation of angular momentum, where operator of angular momentum L and exponential angle operator $E = e^{-i\phi}$

obey the Lie algebra $\mathfrak{e}(2)$ of the Euclidean group in the plane $E(2)$, $[E, L] = E$ [9, 10]. Such observables are related by the Discrete-Continuous Fourier transformation with the all consequences for quantum metrology and phase-space representation [11]. In spite of certain similarities between both the models, there are also significant differences stemming from the fact that formalism of quantum rotor represents the model beyond the harmonic oscillator [12].

The purpose of this Article is driven by possible applications and has two objectives - to investigate and compare possible performance measures used for quantification of uncertainties of complementary variables, and to identify the physical models described by the operators comprising the $\mathfrak{e}(2)$ algebra. The lack of saturable uncertainties is one of the reasons why the angular variable was considered as "problematic". For harmonic oscillator both the constructions adopting either variational approach or commutation rule tend to the same uncertainty relation. For the quantum rotor there is an option to use dispersion or the measure constructed from the covariance matrix of the exponential operator E . Though the uncertainties are not identical, they will yield consistent metrological consequences for optimal measurement. We provide in this paper a remarkable unified interpretation of both measures by extending the \mathbb{R}^2 plane, which is the obvious setting for the analysis of systems with one angle and one angular momentum, to the full \mathbb{R}^3 space. This interpretation comes by considering the measures as moments of inertia of an inhomogeneous ring about axes passing through its center of mass, but with rotations no longer necessarily limited to the original \mathbb{R}^2 plane. In this formulation, the moment of inertia tensor is given by a covariance matrix. Although this extension to 3D is apparently ad hoc, it is extremely advantageous from a metrological perspective as it can be used to formulate new tighter bounds if there is an experimental demand for this. We specify several physical models documenting the interdisciplinary role of quantum rotor: superconducting circuits with Josephson junction - a promising platform for quantum computation. Here the canonical pair of number of Cooper pairs tunneling through Josephson junction and magnetic flux in the super-conducting circuits [13, 14], shaping of optical pulses in

* mista@optics.upol.cz

† matousmista@seznam.cz

‡ hradil@optics.upol.cz

1D described by the Fourier series. The canonical pair corresponds to discrete modal index and continuous time variable. As the last example, let us mention beams with orbital angular momentum [15–17], which provide exquisite experimental platform for quantum information processing in higher dimension with several pivotal experiments [18, 19]. All these examples of quantum rotor-like systems may profit from theory which allows to quantify complementarity of conjugated variables of angular momentum and exponential angle variable.

Historically the concept of angular momentum and angle is regarded as "problematic" from several reasons, some of which we mention here. The misunderstanding can be related to periodicity, due to which the variance is not a good statistical measure since it is not shift invariant. Second, the uncertainties can be relatively easily formulated for sine or cosine of angular variable, as it was done in early days of quantum optics [20, 21]; however these inequalities cannot be saturated simultaneously and therefore extremal state cannot be fully exploited for metrological purposes. As a final example, the problem of angle and angular momentum was plagued by possible ambiguities in theoretical formulation; indeed, the quantum mechanics on the circle can be consistently formulated by means of variables where conjugated variables are combined in rather nontrivial ways [22]. Here the extremal states are the so called "wrapped Gaussian states" - eigenstates of the operator $X = Ee^{-L-1/2}$, which however does not close on an algebra when combined with its conjugate operator. The thorough overview of theoretical concepts linked to angular momentum and angular variable can be found in [9, 23]. For all these reasons the quantum rotor was not considered in applications on an equal footing with the harmonic oscillator, though there are profound analogies in the mathematical description, stemming from the similarities between Fourier transformation and Fourier series [11].

In Sec. II we review concepts for saturable uncertainty relations and extremal states for quantum rotor formulated in various contexts within several decades. Special attention will be paid to arguments based on variational principle and Robertson-like approach. In comparison with analogous theory for quadrature operators, there are subtle but substantial differences in case of quantum rotor. In Sec. III we unify both approaches on an equal footing introducing the moment of inertia. Importantly such a formulation not only unifies existing approaches but gives an opportunity to formulate new and tight uncertainties tailored to possible applications. In Sec. IV we extend the formulation to the problem of simultaneous optimal detection of non-commuting variables, which may find applications extended beyond its mechanical interpretation. Sec. V provides valuable examples where the generic theory developed here can be used including vortex beams, qubits in super-conducting circuits or optimal pulse shaping. Conclusions in Sec. VI summarize all the results stressing the metrological meaning of extremal states as fully fledged minimum uncertainty states for possible metrological applications. Technical calculations related to simplified derivation for generic moment of inertia and ultimate uncertainty relations for correlation matrix are reported in appendices.

II. UNCERTAINTY RELATIONS FOR QUANTUM ROTOR

The theory below is motivated by investigation of uncertainties of two complementary variables. The essence of the theory can be motivated by analogous formulation for position and momentum. The minimum uncertainty states can be derived either by variation or with the help of Schrödinger-Robertson inequality $\langle(\Delta x)^2\rangle\langle(\Delta p)^2\rangle \geq \frac{\hbar^2}{4}$.

- (i) Consider the example of the sum of weighted variances

$$H = \lambda_x(x - \langle x \rangle)^2 + \lambda_p(p - \langle p \rangle)^2. \quad (1)$$

We can consider this as a Hamiltonian of the harmonic oscillator. Its minimum mean value is reached for state corresponding to the projection into the lowest eigenvalue state - squeezed vacuum state, displaced by all possible values $\langle x \rangle, \langle p \rangle$. Such states provide over-complete set of (generalized) coherent states.

- (ii) On the other hand the same solution can be obtained by an alternative way by adopting the uncertainties

$$\begin{aligned} \langle H \rangle &= \lambda_x \langle (\Delta x)^2 \rangle + \lambda_p \langle (\Delta p)^2 \rangle \\ &\stackrel{1}{\geq} 2\sqrt{\lambda_x \lambda_p} \sqrt{\langle (\Delta x)^2 \rangle \langle (\Delta p)^2 \rangle} \stackrel{2}{\geq} \hbar \sqrt{\lambda_x \lambda_p}. \end{aligned} \quad (2)$$

The inequality 1 is saturated by matching the conditions $\lambda_x \langle (\Delta x)^2 \rangle = \lambda_p \langle (\Delta p)^2 \rangle$, whereas inequality 2 is the well-known Robertson inequality. As before the minimum uncertainty states are (squeezed) coherent states.

Both constructions yield the same results for harmonic oscillator, but will deviate for quantum rotor. Minimum uncertainty states play a crucial role in the concept of simultaneous measurement, which is in case of quadrature operators linked with commuting pair $\mathcal{X} = x_s + x_a$, $\mathcal{P} = p_s - p_a$, $[\mathcal{X}, \mathcal{P}] = 0$, known also as the EPR pair. When the measurement is done on a factorized signal and ancillary system, the optimal uncertainty product $\langle(\Delta \mathcal{X})^2\rangle\langle(\Delta \mathcal{P})^2\rangle \geq \hbar^2$ reaches its minimum if local uncertainties are equal $\langle(\Delta x_s)^2\rangle = \langle(\Delta x_a)^2\rangle = \langle(\Delta p_s)^2\rangle = \langle(\Delta p_a)^2\rangle$. The differences between the harmonic oscillator and the rotor are subtle but appear to be essential.

Here, we are interested in a pair of angular momentum operator $L = -i\partial_\phi$ and unitary exponential operator $E = e^{-i\phi}$ satisfying the commutation rule [9, 10]

$$[E, L] = E \quad (3)$$

of Euclidean algebra $e(2)$. In order to formulate uncertainties for angular momentum and angular variable (L, ϕ) , notice that the standard variance $(\Delta\phi)^2$ is not a good uncertainty measure since it is not shift invariant. Statistical dispersion

$$D^2 = \langle \Delta E^\dagger \Delta E \rangle = 1 - |\langle E \rangle|^2 \quad (4)$$

represents the simplest choice of the figure of merit including higher order moments of the "angular variable", not just its variance $(\Delta\phi)^2$. However, as will be seen from the following the angular variable itself will be avoided in favour of exponential angle operator.

The states minimising the variance of angular momentum under the constraint of fixed dispersion (minimum uncertainty states for dispersion) can be sought in the form of variational problem [24] for minimum eigenvalue of the operator

$$\left[L^2 + \mu L + \frac{1}{2}(q^* E + q E^\dagger) \right] |\Psi\rangle = a |\Psi\rangle, \quad (5)$$

with μ, q Lagrange multipliers. The solution is given by Mathieu function [25] in ϕ - representation - even (cos-like) Mathieu function $ce_0(\frac{\phi}{2}, q)$ for its minimum eigenvalue. The minimum uncertainty state thus represents the analogy of vacuum state of the harmonic oscillator. Let us denote formally such a state as $|ce_0, q\rangle$ for $\langle L \rangle = 0$. Even if there is no analytical solution in terms of simple algebraic functions, the bound $B(D)$ can be calculated numerically [24, 26, 27]

$$\langle (\Delta L)^2 \rangle D^2 \geq B(D). \quad (6)$$

The bound $B(D)$ is depicted by the solid red line in Fig. 3. However, the Mathieu ground state can be very closely approximated by the von Mises state $|m, \alpha, \kappa\rangle$ with $m = 0$ and $\alpha = 0$, where in ϕ -representation one has [24, 26]

$$\langle \phi | m, \alpha, \kappa \rangle = \frac{1}{\sqrt{2\pi I_0(2\kappa)}} e^{im\phi + \kappa \cos(\phi - \alpha)}, \quad (7)$$

$\kappa \geq 0$ being a parameter analogous to squeezing in close analogy with formulation for quadrature operators. Differences between ground Mathieu and von Mises states are so small (compare solid red line and dashed blue line in Fig. 3) that hardly can be observed by current technology and due to this, we will replace this analytically intractable bound $B(D)$ by its good approximation in terms of von Mises states. Explicit form can be easily found with the help of formulae derived in [11] in parametric form depending on κ

$$\langle (\Delta L)^2 \rangle D^2 = \frac{\kappa}{2} \frac{I_1(2\kappa)}{I_0(2\kappa)} \left[1 - \frac{I_1^2(2\kappa)}{I_0^2(2\kappa)} \right], \quad (8)$$

$$D^2 = 1 - \frac{I_1^2(2\kappa)}{I_0^2(2\kappa)}. \quad (9)$$

There are physical reasons why Mathieu and von Mises ground states are so closely related. Whereas the Mathieu ground state minimises the uncertainty product for dispersion and variance of angular momentum, von Mises states are extremal states for uncertainty product of angular momentum and exponential angle operator. Indeed the commutation relations for rotated sine and cosine operators

$$[S_\alpha, L] = iC_\alpha, \quad (10)$$

$C_\alpha = (e^{-i\alpha} E^\dagger + e^{i\alpha} E)/2$, $S_\alpha = (e^{-i\alpha} E^\dagger - e^{i\alpha} E)/2i$, yields the uncertainty relation

$$\langle (\Delta L)^2 \rangle \langle (\Delta S_\alpha)^2 \rangle \geq \frac{1}{4} |C_\alpha|^2, \quad (11)$$

which is saturated by the von Mises states (7) - the solution of the operator equation

$$(\Delta L - i\kappa \Delta S_\alpha) |\psi\rangle = 0. \quad (12)$$

The saturable bounds as a function of covariance matrix can be derived by an approach inspired by Ref. [28]. Let us introduce a normalised variable vector $\mathbf{x} = (\cos \alpha, \sin \alpha)^T$, an unnormalised vector of the first moments $\mathbf{c} = (\langle C \rangle, \langle S \rangle)^T$, and the covariance matrix

$$\mathbf{\Gamma} = \begin{pmatrix} \langle (\Delta S)^2 \rangle & -\frac{1}{2} \langle \{\Delta S, \Delta C\} \rangle \\ -\frac{1}{2} \langle \{\Delta S, \Delta C\} \rangle & \langle (\Delta C)^2 \rangle \end{pmatrix}, \quad (13)$$

where $\{A, B\} \equiv AB + BA$ is the anticommutator. Hence, we get

$$\langle C_\alpha \rangle = \mathbf{c}^T \mathbf{x}, \quad \langle (\Delta S_\alpha)^2 \rangle = \langle [\Delta(S \cos \alpha - C \sin \alpha)]^2 \rangle = \mathbf{x}^T \mathbf{\Gamma} \mathbf{x}, \quad (14)$$

and the uncertainty relation (11) takes the form

$$\langle (\Delta L)^2 \rangle (\mathbf{x}^T \mathbf{\Gamma} \mathbf{x}) \geq \frac{1}{4} (\mathbf{c}^T \mathbf{x})^2. \quad (15)$$

Moving all the quantities dependent on angle α , i.e., on the unit vector \mathbf{x} , to the right-hand side (RHS) of the uncertainty relation, we can maximise the RHS over the vector \mathbf{x} thereby getting [28],

$$\langle (\Delta L)^2 \rangle \geq \frac{1}{4} \max_{\|\mathbf{x}\|=1} \frac{(\mathbf{c}^T \mathbf{x})^2}{(\mathbf{x}^T \mathbf{\Gamma} \mathbf{x})} = \frac{1}{4} \frac{(\mathbf{c}^T \mathbf{x}_0)^2}{\mathbf{x}_0^T \mathbf{\Gamma} \mathbf{x}_0} = \frac{1}{4} \mathbf{c}^T \mathbf{\Gamma}^{-1} \mathbf{c}, \quad (16)$$

where $\mathbf{x}_0 = \mathbf{J} \mathbf{\Gamma} \mathbf{J}^T \mathbf{c} / \sqrt{\mathbf{c}^T \mathbf{J} \mathbf{\Gamma}^2 \mathbf{J}^T \mathbf{c}}$, $\mathbf{J} = i\sigma_y$, is the unit vector for which the maximum on the RHS is reached. As a result the following chain of inequalities can be derived

$$\langle (\Delta L)^2 \rangle \geq \frac{1}{4} \frac{(\mathbf{c}^T \mathbf{x}_0)^2}{(\mathbf{x}_0^T \mathbf{\Gamma} \mathbf{x}_0)} \geq \frac{1}{4} \frac{\|\mathbf{c}\|^2}{\mathbf{m}^T \mathbf{\Gamma} \mathbf{m}} \geq \frac{1}{4} \frac{\|\mathbf{c}\|^2}{\gamma_+} \geq \frac{1}{4} \frac{\|\mathbf{c}\|^2}{D^2}, \quad (17)$$

where $\|\mathbf{c}\|^2 = \langle E \rangle^2$ and $\mathbf{m} = \mathbf{c}/\|\mathbf{c}\|$. Inequality 1 is given in (16), inequality 2 follows from the Cauchy-Schwarz inequality

$$(\mathbf{m}^T \mathbf{\Gamma} \mathbf{m})(\mathbf{m}^T \mathbf{\Gamma}^{-1} \mathbf{m}) \geq 1, \quad (18)$$

inequality 3 trivially estimates the mean value of covariance matrix by the larger eigenvalue γ_+ ,

$$\gamma_\pm = \frac{1}{2} (1 - \langle E \rangle^2 \pm \langle E^2 \rangle - \langle E \rangle^2),$$

and inequality 4 originally proposed in [20] (see also [21]) cannot be saturated except for $D = 0$.

The denominators $\mathbf{x}_0^T \mathbf{\Gamma} \mathbf{x}_0$, $\mathbf{m}^T \mathbf{\Gamma} \mathbf{m}$ and γ_+ appearing on the right-hand sides of the chain of inequalities (17) represent possible alternative uncertainty measures of angular variable constructed from elements of the covariance matrix (13). These measures coincide for von Mises states, $\mathbf{x}_0^T \mathbf{\Gamma} \mathbf{x}_0 = \mathbf{m}^T \mathbf{\Gamma} \mathbf{m} = \gamma_+$, and all the inequalities 1, 2 and 3 reduce to equalities. However, the measures are not the same for other than extremal states, since they are forged from different parameters of covariance matrix. The least one is $\mathbf{x}_0^T \mathbf{\Gamma} \mathbf{x}_0$ and it is on the RHS of inequality 1 but the simplest one is given on the RHS of inequality 2 and it was heuristically derived in

[11], $\mathbf{m}^T \mathbf{\Gamma} \mathbf{m} = \langle S_{-\arg(E)}^2 \rangle$. Note finally that the quantities $\mathbf{x}_0^T \mathbf{\Gamma} \mathbf{x}_0$ and $\mathbf{m}^T \mathbf{\Gamma} \mathbf{m}$ are ill-defined for states with $\langle E \rangle = 0$, i.e., $\mathbf{c} = (0, 0)^T$, in which case we define both of them as $\gamma_- = (1 - |\langle E^2 \rangle|)/2$.

In the next section we show that concept of moment of inertia unifies all the concepts analysed above, and allows to design tighter uncertainty relations.

III. MOMENTS OF INERTIA AS THE ANGULAR UNCERTAINTY MEASURES

Let us review briefly the notion of the moment of inertia tensor from classical mechanics. Consider a rigid body of volume V and mass density ρ that rotates with angular velocity vector $\boldsymbol{\omega}$ along a fixed axis passing through a point A . The mass element $dm = \rho dV$ with a position vector \mathbf{r} relative to the point A has the velocity vector $\mathbf{v} = \boldsymbol{\omega} \times \mathbf{r}$. The angular momentum and the energy of the body then can be cast in the form

$$\mathbf{L}_A = \int_V [\mathbf{r} \times \mathbf{v}] \rho dV = \mathbf{I}_A \boldsymbol{\omega}, \quad (19)$$

$$E = \frac{1}{2} \boldsymbol{\omega}^T \cdot \mathbf{L}_A = \frac{1}{2} \boldsymbol{\omega}^T \mathbf{I}_A \boldsymbol{\omega}, \quad (20)$$

where \mathbf{I}_A is the moment of inertia tensor with respect to the point A , which is defined by the matrix

$$\mathbf{I}_A = \begin{pmatrix} \int_V (y^2 + z^2) \rho dV & -\int_V xy \rho dV & -\int_V xz \rho dV \\ -\int_V xy \rho dV & \int_V (x^2 + z^2) \rho dV & -\int_V yz \rho dV \\ -\int_V xz \rho dV & -\int_V yz \rho dV & \int_V (x^2 + y^2) \rho dV \end{pmatrix}. \quad (21)$$

Now, let the body be a unit ring in the $X - Y$ plane, centered at the origin O . Assume further the ring to have a unit mass distributed along the ring with the angular mass density $p(\phi)$. From the definition (21) it then follows that the moment of inertia tensor of the ring about the origin O is given by

$$\mathbf{I}_O = \begin{pmatrix} \langle S^2 \rangle & -\langle SC \rangle & 0 \\ -\langle SC \rangle & \langle C^2 \rangle & 0 \\ 0 & 0 & 1 \end{pmatrix}, \quad (22)$$

where we introduced the denotation $\langle S^2 \rangle = \langle \sin^2(\phi) \rangle$, $\langle C^2 \rangle = \langle \cos^2(\phi) \rangle$, and $\langle SC \rangle = \langle \sin(\phi) \cos(\phi) \rangle$. Recall further the parallel axis theorem connecting the moment of inertia tensor with respect to a point A and the center of mass G ,

$$\mathbf{I}_A = \mathbf{I}_G + m(\mathbf{a}^2 \mathbf{1} - \mathbf{a} \mathbf{a}^T), \quad (23)$$

where \mathbf{a} is the position vector of the point G relative to the point A .

Moving back to the ring, we have $\mathbf{a} = (\langle C \rangle, \langle S \rangle, 0)^T$ and the theorem (23) implies

$$\mathbf{I}_G = \begin{pmatrix} \mathbf{\Gamma} & 0 \\ 0 & D^2 \end{pmatrix}, \quad (24)$$

where $\mathbf{\Gamma}$ is the covariance matrix defined in Eq. (13). Hence, the moment of inertia of the ring about an axis determined by

a unit vector $\mathbf{n} = (n_x, n_y, n_z)^T$ and passing through its center of mass G is given by

$$M_{\mathbf{n}} = \mathbf{n}^T \mathbf{I}_G \mathbf{n} = \mathbf{n}_{xy}^T \mathbf{\Gamma} \mathbf{n}_{xy} + D^2 n_z^2, \quad (25)$$

where $\mathbf{n}_{xy} = (n_x, n_y)^T$.

Similarity of the formula (25) with the variance $\langle (\Delta S_a)^2 \rangle = \mathbf{x}^T \mathbf{\Gamma} \mathbf{x}$, Eq. (14), brings us to the idea to interpret all the angular uncertainty measures of the preceding section as moments of inertia of a ring about axes passing through its center of mass. The mechanical interpretation and the geometrical meaning of some of the measures is depicted in Figs. 1 and 2. Specifically, the dispersion (4) can be interpreted as a moment of inertia of the ring about an axis perpendicular to its plane, i.e., parallel with the unit vector $\mathbf{e}_z = (0, 0, 1)^T$, and passing through its center of mass [29] (see Fig. 1 and the red axis in Fig. 2).

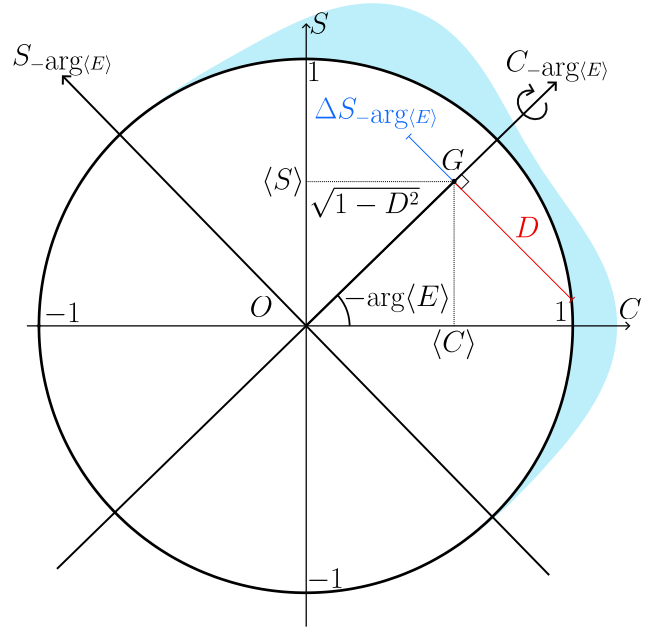


FIG. 1. Geometrical and mechanical meaning of angular uncertainty measures for mixture $\rho = 0.4|0, 0\rangle\langle 0, 0| + 0.6|0, 2\pi/5\rangle\langle 0, 2\pi/5|$ of two von Mises states with the same parameter $\kappa = 5$. The probability density $p(\phi) = \langle \phi | \rho | \phi \rangle$ (light blue area) can be viewed as a linear mass density of an inhomogeneous unit ring with unit mass (black ring). The point $G(\langle C \rangle, \langle S \rangle)$ is the center of mass of the ring. The dispersion D^2 (square of the red line segment) is the moment of inertia $M_{\mathbf{e}_z}$, Eq. (26), of the ring about an axis perpendicular to its plane and passing through G (see the red axis in Fig. 2). The variance $\langle (\Delta S_{-\arg(E)})^2 \rangle$ (square of the blue line segment) is the moment of inertia $M_{\mathbf{e}}$, Eq. (27), of the ring about the axis $C_{-\arg(E)}$.

This can be easily seen without any calculations in the frame rotated by an angle $-\arg(E)$ since the position of the center of mass is on the line $\langle S_{-\arg(E)} \rangle = 0$ at the distance $\langle C_{-\arg(E)} \rangle = |\langle E \rangle| = \sqrt{1 - D^2}$ from the origin (see Fig. 1). The moment of inertia of the ring with respect to the origin equals to 1 and the moment of inertia with respect to the center of mass is given by the parallel axis theorem as

$$M_{\mathbf{e}_z} = 1 - \langle C_{-\arg(E)} \rangle^2 = D^2. \quad (26)$$

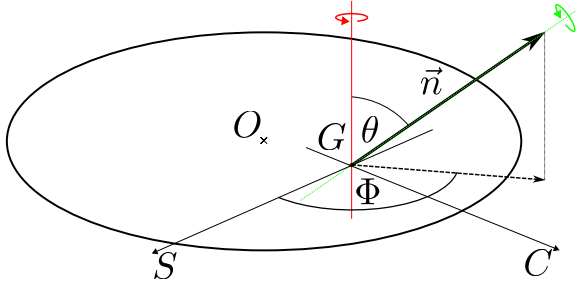


FIG. 2. Mechanical interpretation of the dispersion D^2 , Eq. (26), and the generic angular uncertainty measure $M_{\mathbf{n}}$, Eq. (28). The dispersion is the moment of inertia of the ring with respect to the red axis. The measure $M_{\mathbf{n}}$ is the moment of inertia of the ring about the green axis determined by the unit vector $\mathbf{n} = (\sin \theta \cos \Phi, \sin \theta \sin \Phi, \cos \theta)$. See text and caption of Fig. 1 for details.

Analogously, the uncertainty measure in (17)

$$M_{\mathbf{e}} = \langle S_{-\arg(E)}^2 \rangle \quad (27)$$

represents the moment of inertia of the ring with respect to the axis connecting the origin O and the center of mass G , which is determined by the unit vector $\mathbf{e} = (\langle C \rangle, \langle S \rangle, 0)^T / |\langle E \rangle|$ (see axis $C_{-\arg(E)}$ in Fig. 1).

These are the special cases of moment of inertia with respect to the axis at the center of mass and oriented along the unit vector $\mathbf{n} = (\sin \theta \cos \Phi, \sin \theta \sin \Phi, \cos \theta)$ (see green axis in Fig. 2). A straightforward substitution into the formula (25) gives the result

$$M_{\mathbf{n}} = \langle (\Delta S_{\Phi})^2 \rangle + \cos^2(\theta) \langle (\Delta C_{\Phi})^2 \rangle = D^2 - \sin^2(\theta) \langle (\Delta C_{\Phi})^2 \rangle. \quad (28)$$

It is intriguing to note that variances used for quantification of uncertainties of position and momentum are nothing but moments of inertia of a probability distribution along the line (1D) with respect to perpendicular axis in the center of mass.

Note further that the quantity (28) is obviously equipped with some of the formal properties of an uncertainty measure as formulated in [30]. Namely, it is non-negative and for the state-independent angles Φ and θ it is obviously well defined and concave. Here, the concavity simply follows from concavity of variance [31] or from the fact that the measure is related to the moment of inertia tensor. To show the latter, consider the convex mixture $\rho = p\rho_1 + (1-p)\rho_2$, and let I_G, I_{G_1} , and I_{G_2} be the moment of inertia tensors with respect to the center of mass corresponding to the density matrices ρ, ρ_1 and ρ_2 . Then it is not difficult to show that

$$\mathbf{I}_G = p\mathbf{I}_{G_1} + (1-p)\mathbf{I}_{G_2} + p(1-p)(R^2\mathbf{1} - \mathbf{R}\mathbf{R}^T), \quad (29)$$

where $\mathbf{R} = (\langle C \rangle_{\rho_2} - \langle C \rangle_{\rho_1}, \langle S \rangle_{\rho_2} - \langle S \rangle_{\rho_1}, 0)^T$ is the position vector of the center of mass G_2 with respect to the center of mass G_1 . Hence, one gets immediately concavity of the measure (28),

$$M_{\mathbf{n}}(\rho) \geq pM_{\mathbf{n}}(\rho_1) + (1-p)M_{\mathbf{n}}(\rho_2), \quad (30)$$

where the Cauchy-Schwarz inequality $R^2 \geq |(\mathbf{n}^T \cdot \mathbf{R})|^2$ has been used.

How to understand all those results in the context of possible metrological applications? Moment of inertia is well defined quantity associated with the rotation of a rigid body. According to the inequalities (6) and (17) moments of inertia, namely $D^2 \geq \gamma_+ \geq \mathbf{m}^T \mathbf{\Gamma} \mathbf{m} \geq \mathbf{x}_0^T \mathbf{\Gamma} \mathbf{x}_0$ play the role of the "uncertainties" of the angular variable. Obviously, dispersion as moment of inertia (26) seems to be the first choice but the Mathieu states are analytically intractable and cannot be fully exploited for further optimization. On the other hand measures constructed from higher order moments (17) and linked to moment of inertia (27) may seem to be forged "artificially" but give rise to a simple tractable set of extremal von Mises states, which are effectively indistinguishable from Mathieu states. In the line with this interpretation the inequalities (6) and (17) cannot be seen as "stronger" or "weaker" since different measures are involved. However, both concepts, though "slightly" different seem to be equivalent for all practical consequences and, all measures implied by inequalities (17) are mimicking dispersion when considering states close to optimal. Of course, differences may appear for "non-optimal" states due to the differences in higher order moments.

It follows from this argument that states saturating the Robertson's inequality are "minimum uncertainty states" if the concept of uncertainty is extended to projections of moment of inertia tensor with state-dependent orientation of axis of rotation: variance of sine (cosine) operator or dispersion are just extremal cases of more general formulae (28). Dispersion as a measure is in this sense exceptional since the axis is constant (perpendicular to $X - Y$ plane). Why is it worth to have some "other" uncertainty relations? The answer is simple: They can characterise extremal states under different conditions and may provide tighter uncertainty relations! The tight form of generic uncertainty relations is formulated in Appendix B as an open problem, the solution of which is not an easy task. Here we will just stress pragmatical reasons why this could be of interest: If some particular physical platform of quantum rotor (see below) will allow to identify experimentally moments of angular variable $\langle E \rangle$ and $\langle E^2 \rangle$, it could be valuable to find restrictions implied by quantum mechanics and to formulate stronger uncertainties. We will leave these issues for further research resorting to the simplest opportunity associated with the measure (27), which may find direct applications.

IV. SIMULTANEOUS DETECTION OF COMPLEMENTARY VARIABLES

The uncertainty relations discussed above have immediate implications for metrology. The angular momentum and angular variable can be detected simultaneously in the extended Hilbert space of a signal (s) and ancillary (a) systems via the commuting pair [11]

$$\mathcal{L} = L_s + L_a, \quad \mathcal{E} = E_s E_a^\dagger, \quad [\mathcal{L}, \mathcal{E}] = 0. \quad (31)$$

It is plausible to assume that commuting pair (31) represents the optimal scheme for any purpose. Here we address just the

strategy based on minimizing the uncertainties. For metrology on signal state the ancillary system is controlled independently from the signal system and the global state is factorised $|\psi\rangle_{sa} = |\varphi\rangle_s |\chi\rangle_a$. Setting the ancillary system to some fiducial state $|f\rangle$, which will be specified later, leads to an over-complete POVM in signal space projecting onto the states $D(m, \phi)|f\rangle$ and satisfying the completeness condition

$$\sum_{m \in \mathbb{Z}} \int_{-\pi}^{\pi} \frac{d\phi}{2\pi} D(m, \phi) |f\rangle \langle f| D^\dagger(m, \phi) = \mathbb{1}, \quad (32)$$

where $D(m, \phi) = e^{-iL\phi} E^{-m}$ is the displacement operator with an arbitrary phase factor being omitted. The choice of the fiducial state dictated by the optimality can be either the ground Mathieu state $|ce_0, q\rangle$, von Mises state $|0, 0, \kappa\rangle$, or other optimal state discussed in previous Section. The figures of merit used to quantify uncertainties of the angular momentum and the angular variable for the commuting pair (31) can be cast in the form

$$\langle (\Delta \mathcal{L})^2 \rangle = \langle (\Delta L_s)^2 \rangle + \langle (\Delta L_a)^2 \rangle, \quad (33)$$

$$\mathcal{D}^2 = 1 - |\langle \mathcal{E} \rangle|^2 = |\langle E_a \rangle|^2 D_s^2 + D_a^2, \quad (34)$$

$$\langle (\Delta \mathcal{S})^2 \rangle = |\langle E_a \rangle|^2 \langle (\Delta S_s)^2 \rangle + \langle (\Delta S_a)^2 \rangle. \quad (35)$$

The quantity on the left-hand side of Eq. (35) is defined as $\Delta \mathcal{S} = \mathcal{S}_{\beta = \arg\langle E_a \rangle - \arg\langle E_s \rangle}$, where $\mathcal{S}_\beta = (e^{-i\beta} \mathcal{E}^\dagger - e^{i\beta} \mathcal{E})/2i$, and the RHS has been obtained under the assumptions $\arg\langle E_a \rangle = 0$, $\arg\langle E_s \rangle = 0$, which suppress the unwanted influence of the ancilla on the measurement outcomes [11].

Simultaneous detection exhibits added noise in both angular momentum and angular variable, but the latter one is penalized by an extra multiplicative factor $|\langle E_a \rangle|^2$ or $|\langle E_s \rangle|^2$, Eqs. (34) and (35), respectively, a consequence of the fact that the angular variable is always measured with respect to a reference.

Full analysis of optimal simultaneous detection is a delicate task, which depends on constraints. Just to get the flavour we will specify two opposite scenarios, namely to optimize ancilla state for a given signal state or conversely, to optimize signal state for a given ancilla state. The first task is more involved since it requires to consider measurements which depend on the measured signal - a situation which frequently happens when Quantum Fisher information is considered. Here we address the second task, which has a straightforward metrological meaning answering the question what signal is optimally detected by a given apparatus (ancilla). Detailed discussions will be done here for dispersion, the analogous arguments for $\langle (\Delta \mathcal{S})^2 \rangle$ can be found in Appendix C. The analysis is facilitated by introducing the vector notation

$$\boldsymbol{\ell} = (\Delta L_s, \Delta L_a)^\top, \quad \mathbf{d}_{ij} = (|\langle E_i \rangle| D_j, D_i)^\top, \quad (36)$$

where $i, j = a, s$, and $\Delta A \equiv \sqrt{\langle (\Delta A)^2 \rangle}$. The essence of the analysis is to find several branches which saturate the uncertainty relations and this is achieved by reordering the terms in the vector \mathbf{d}_{ij} . As a result the uncertainty product can be

assessed as

$$\begin{aligned} \Pi_{\mathcal{D}} &= \langle (\Delta \mathcal{L})^2 \rangle \mathcal{D}^2 = \|\boldsymbol{\ell}\|^2 \|\mathbf{d}_{ij}\|^2 \stackrel{1}{\geq} |\langle \boldsymbol{\ell}^\top \cdot \mathbf{d}_{ij} \rangle|^2 \\ &= \begin{cases} (\langle E_s \rangle |\Delta L_s D_a + \Delta L_a D_s|)^2 & \text{for } ij = sa; \\ (\langle E_a \rangle |\Delta L_s D_s + \Delta L_a D_a|)^2 & \\ \stackrel{2}{\geq} (|\langle E_a \rangle| \sqrt{B_s} + \sqrt{B_a})^2 & \text{for } ij = as, \end{cases} \quad (37) \end{aligned}$$

where inequality 1 follows from the Cauchy-Schwarz inequality, whereas inequality 2 is a consequence of the uncertainty relation (6). The rationale behind the mathematical formulation stems from the fact that separate uncertainties $\langle (\Delta \mathcal{L})^2 \rangle$ and \mathcal{D}^2 can be interpreted as norms of vectors, for which the Cauchy-Schwarz inequalities represent saturable bounds with several possible branches. The analysis hinges partially on numerical analysis due to the dependence on the state-dependent factor $\langle E_a \rangle$. The results are summarized in Fig. 3. In Appendix C 1 we show further that the numerically found optimal value of the uncertainty product $\Pi_{\mathcal{D}}$ can be well approximated for ancilla prepared in the Mathieu state as $\mathcal{B}_{\mathcal{D}}$,

$$\mathcal{B}_{\mathcal{D}} = \begin{cases} (|\langle E_a \rangle| \sqrt{B_s} + \sqrt{B_a})^2 & \text{for } D_{a,\text{int}}^2 > D_a^2 \geq 0; \\ \langle (\Delta L_a)^2 \rangle & \text{for } 1 \geq D_a^2 \geq D_{a,\text{int}}^2, \end{cases} \quad (38)$$

where $D_{a,\text{int}}^2 \doteq 0.3$. The derivation was done here for dispersion and Mathieu extremal states but analogous formulation done for the uncertainty measure $\langle (\Delta \mathcal{S})^2 \rangle$, Eq. (35), and von Mises states (see Fig. 4) shows the consistency of both the measures. In Appendix C 2 we show further that the optimal numerical bound is very well approximated by the function

$$\mathcal{B}_{\mathcal{S}} = \begin{cases} \frac{1}{4} \left(\sqrt{|\langle E_a \rangle|^2} |\langle E_s \rangle| + |\langle E_a \rangle| \right)^2 & \text{for } \tilde{D}_{a,\text{int}}^2 > D_a^2 \geq 0; \\ \frac{\langle (\Delta L_a)^2 \rangle}{2} & \text{for } 1 \geq D_a^2 \geq \tilde{D}_{a,\text{int}}^2, \end{cases} \quad (39)$$

where $\tilde{D}_{a,\text{int}}^2 \doteq 0.167$ and the parameters of the signal and ancilla are matched by the condition $\kappa_s = \sqrt{I_2(2\kappa_a)/I_0(2\kappa_a)} \kappa_a$ [11]. This result has clear interpretation as condition matching the "squeezing" of signal and ancillary systems. Notice in passing that for x and p quadrature operators of the harmonic oscillator both signal and ancillary systems are squeezed equally.

Disregarding the subtle differences between von Mises and Mathieu extremal states and optimal conditions for matching signal and ancillary systems, the "almost optimal" simultaneous detection of complementary variables can be seen as detection of the von Mises signal state projected onto sequence of von Mises detector states (32) - a result fully analogous to the heterodyne detection for harmonic oscillator when squeezed state can be measured by projecting into squeezed (Gaussian) states. However the structure of "optimal conditions" is much richer for quantum rotor with promises for future experimental realisations.

V. QUANTUM ROTOR IN APPLICATIONS

There are several distinct and important physical platforms for implementing quantum rotor in the current technology.

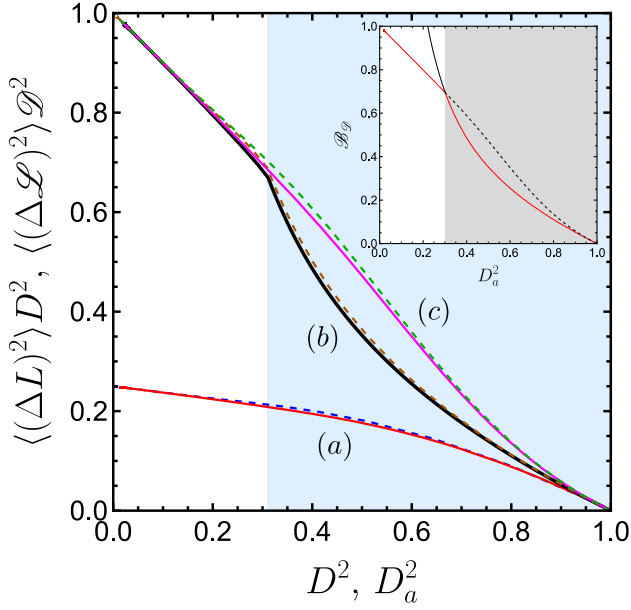


FIG. 3. Uncertainty product $\langle(\Delta L)^2\rangle D^2$ as a function of dispersion D^2 (a) and $\Pi_{\mathcal{D}} = \langle(\Delta \mathcal{L})^2\rangle \mathcal{D}^2$ as a function of D_a^2 (b), (c). The products are plotted for the extremal Mathieu states $|\text{ce}_0, q\rangle$ (solid lines) and the von Mises states $|0, 0, \kappa\rangle$ (dashed lines). The pair of lines (a) shows that the von Mises states approximate the optimal Mathieu states very closely and this correspondence propagates into simultaneous measurement under various strategies. The pair of lines (b) corresponds to the numerical solutions with optimally matched Mathieu and von Mises states, and in case of (c) the signal is matched to ancilla according to the conditions saturating the Cauchy-Schwarz inequality. The inset displays the function $\mathcal{B}_{\mathcal{S}}$ characterizing minimal $\Pi_{\mathcal{D}}$ (solid red line) and the remaining parts of its two branches (black lines). The branches give analytical arguments explaining the numerical solution.

Detailed analysis of specific examples is beyond the scope of this contribution. Here we just point out common features of all the examples, namely that uncertainties for complementary variables represent the first step towards optimal metrology. Note in passing the obvious example of systems with cylindrical symmetry, namely vortex beams, which was already discussed in Ref. [24], where the bounds for dispersion and variance of angular momentum were verified experimentally. It is intriguing to note that exponential angle operator can be constructed on 2 modes of transversal field associated with annihilation operators a_1, a_2 as so called "feasible" phase [32]

$$L = a_1^\dagger a_1 - a_2^\dagger a_2, \quad E = \sqrt{\frac{a_1 + a_2^\dagger}{a_1^\dagger + a_2}}. \quad (40)$$

As shown by Ban [33], there is an equivalent formulation of this problem in terms of relative number state representation. These concepts come from formal considerations of "quantum phase operator" and provide exact (and intrinsically nonlinear) link between algebra of harmonic oscillator and quantum rotor.

Less obvious is the link between the problem of optimal

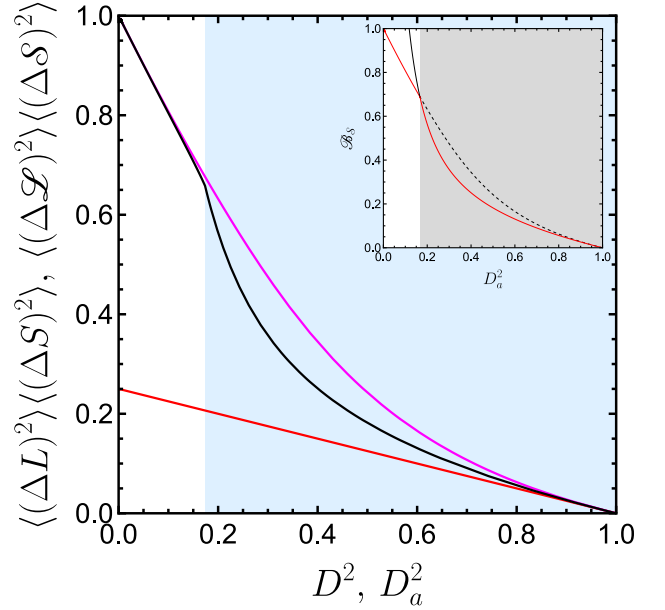


FIG. 4. Uncertainty product $\langle(\Delta L)^2\rangle \langle(\Delta S)^2\rangle$ as a function of dispersion D^2 (red line) and $\Pi_{\mathcal{S}} = \langle(\Delta \mathcal{L})^2\rangle \langle(\Delta \mathcal{S})^2\rangle$ as a function of D_a^2 . The products are plotted for the extremal von Mises states $|0, 0, \kappa\rangle$. The black line corresponds to the numerical solutions with optimally matched von Mises states, and the magenta line depicts the case when the signal is matched to ancilla according to the conditions saturating the Cauchy-Schwarz inequality. The inset displays the function $\mathcal{B}_{\mathcal{S}}$ characterizing minimal $\Pi_{\mathcal{S}}$ (solid red line) and the remaining parts of its two branches (black lines).

shaping of the pulse in the time-frequency domain and the model of a quantum rotor. For the sake of simplicity we assume t-dependent signal on the 2π window in dimensionless coordinates, where t plays the role of angular variable. Outside this interval let us fulfill for simplicity the periodicity condition $\psi(t + 2\pi) = \psi(t)$. Such signals can be represented by discrete Fourier series in the selected time window

$$\psi(t) = \sum_{n=-\infty}^{\infty} a_n e^{in}. \quad (41)$$

If we define operators in t-representation as $L = -i\partial_t$, $E = e^{-it}$, we easily identify the commutation relation for $\mathfrak{e}(2)$ algebra (3) with all the metrological consequences. In contrast with the "standard" formulation where x, p are related by Fourier transformation, the discrete n and continuous t -variables are parameters in Fourier series. This problem will be addressed in a subsequent publication.

Contemporary quantum computing platforms for performing quantum operations are on circuits with Josephson junctions. Superconductors behave like macroscopic quantum mechanical systems. Only two quantities are required to describe the physics of a Josephson junction: the number imbalance of electrons n (Cooper pairs) and θ is the relative phase between the two superconductors. The circuits built with superconducting components can carry currents without resistance because the carriers of the charge - electrons or holes near

the Fermi energy level - are creating the Cooper pairs creating macroscopic coherent states as explained by BCS theory. Such a state can be described by complex-valued order parameter, the phase of which is essential for the physics of super-conducting qubits [34]. The standard explanation in solid state physics relies on the canonical pair "[$\hat{\theta}, \hat{n}$]" = i , though it is known that this form is mathematically not rigorous due to the periodicity of angular variable [14, 35, 36]. The quotation marks are indicating the potential problems: the number of Cooper pairs n tunneling through the barrier in Josephson junction can be negative while θ linked with gauge phase over the barrier is periodic, bearing the striking similarity with "phase-number operators". However, the relation $e^{i\theta} n e^{-i\theta} = n - 1$ is free of those problems but this is nothing else but the algebraic expression for Euclidean algebra $e(2)$, Eq. (3), for the exponential operator $E = e^{-i\theta}$. But there are still other analogies linking the uncertainty relations for the quantum rotor. Under the conditions of super-conductivity only Cooper pairs tunnel coherently in the superconducting junction, and the system is described by the Hamiltonian of island-base qubit with capacitance coupled to Josephson junction [34] called also Cooper pair box

$$H = 4E_C(n - n_g)^2 - E_J \cos \theta, \quad (42)$$

where n is number operator for excess Cooper pair charges in the island, θ is the phase of the superconducting order parameter of the island, E_C is the charging energy and E_J is the Josephson junction energy. As pointed out in [35], the Cooper box is to quantum circuit physics what the hydrogen atom is to atomic physics. But this Hamiltonian of a quantum rotor [13] is the same as the extremal equation (5) for states minimising uncertainty for the variance of angular momentum and dispersion (6). In other words, projections into the (displaced) ground state of the quantum rotor have the same meaning for quantum tomography of super-conduction qubits as projections into (displaced) ground state of harmonic oscillator, i.e., projections into squeezed states of electromagnetic field. Since Mathieu states can be very closely approximated by von Mises states the theory presented here provides deep analogy between quantum metrology of harmonic oscillator and quantum rotor. This is facilitated by the generalised measurement of commuting pair (31), where the signal and ancillary loops

should be coupled to more complex circuits allowing to detect super-imposed (or subtracted) complementary variables from both loops. A practical goal of the results presented here could be the design of optimised detection and diagnostics of super-conducting qubits such as charge-, phase- or transmon qubit states [37]. In order to reach such an ambitious goal concentrated effort is surely needed utilising the potential advantages of both quantum harmonic oscillator and rotor.

VI. CONCLUSION

The quantum rotor - the second simplest model of complementary variables after harmonic oscillator is of paramount yet under-appreciated importance in contemporary quantum science. Though rotational symmetry is a well understood concept, insight into the canonical pair of angular momentum and angular variable was obscured by problems stemming from inadequate description of complementary variables and the lack of saturable uncertainty relations. We show that moment of inertia with the probability distributed on the unit ring with respect to various rotation axes going through center of mass can be used for meaningful quantification of angular variable and for the formulation of variations of the uncertainty principle. This unifying approach allows to formulate the metrology of quantum rotor along the lines of those known for harmonic oscillator. Particular attention is paid to relations saturated by Mathieu or von Mises states allowing to formulate concept of optimal detection of complementary variables for system like pulses or super-conducting qubits with Josephson junction. Quantum information processing adopting both basic models of harmonic oscillator and quantum rotor may bring new and challenging ideas for processing of quantum information due to the inherent nonlinearities between both models: what is linear operation for harmonic oscillator is nonlinear for rotor and vice versa.

ACKNOWLEDGMENTS

The authors are indebted to Jaroslav Řeháček and Hubert de Guise for valuable comments. We acknowledge financial support from H2020-FETOPEN-2018-2019-2020-01 Stormy-Tune.

-
- [1] A. Einstein, B. Podolsky, and N. Rosen, "Can quantum-mechanical description of physical reality be considered complete?" *Phys. Rev.* **47**, 777 (1935).
 - [2] E. Arthurs and J. L. Kelly, "B.S.T.J. briefs: On the simultaneous measurement of a pair of conjugate observables," *Bell Syst. Tech. J.* **44**, 725 (1965).
 - [3] S. Stenholm, "Simultaneous measurement of conjugate variables," *Ann. Phys.* **218**, 233 (1992).
 - [4] E. P. Wigner, "On the quantum correction for thermodynamic equilibrium." *Phys. Rev.* **40**, 749 (1932).
 - [5] K. Husimi, "Some formal properties of the density matrix," *Proc. Phys. Math. Soc. Jpn.* **22**, 264 (1940).
 - [6] R. J. Glauber, "Coherent and incoherent states of the radiation field," *Phys. Rev.* **131**, 2766 (1963).
 - [7] S. L. Braunstein and H. J. Kimble, "Teleportation of continuous quantum variables," *Phys. Rev. Lett.* **80**, 869 (1998).
 - [8] F. Grosshans and P. Grangier, "Continuous variable quantum cryptography using coherent states," *Phys. Rev. Lett.* **88**, 057902 (2002).
 - [9] H. A. Kastrup, "Quantization of the canonically conjugate pair angle and orbital angular momentum," *Phys. Rev. A* **73**, 052104

- (2006).
- [10] K. Kowalski and J. Rembieliński, “On the uncertainty relations and squeezed states for the quantum mechanics on a circle,” *J. Phys. A: Math. Gen.* **35**, 1405 (2002).
- [11] L. Mišta Jr., H. de Guise, J. Řeháček, and Z. Hradil, “Angle and angular momentum: Uncertainty relations, simultaneous measurement, and phase-space representation,” *Phys. Rev. A* **106**, 022204 (2022).
- [12] V. V. Albert, S. Pascasio, and M. H. Devoret, “General phase spaces: from discrete variables to rotor and continuum limits,” *J. Phys. A: Math. Theor.* **50**, 504002 (2017).
- [13] J. Koch, M. Y. Terri, J. Gambetta, A. A. Houck, D. I. Schuster, J. Majer, A. Blais, M. H. Devoret, S. M. Girvin, and R. J. Schoelkopf, “Charge-insensitive qubit design derived from the Cooper pair box,” *Phys. Rev. A* **76**, 042319 (2007).
- [14] U. Vool and M. Devoret, “Introduction to quantum electromagnetic circuits,” *Int. J. Circ. Theor. Appl.* **45**, 897 (2017).
- [15] G. Molina-Terriza, J. P. Torres, and L. Torner, “Twisted photons,” *Nat. Phys.* **3**, 305 (2007).
- [16] A. M. Yao and M. J. Padgett, “Orbital angular momentum: origins, behavior and applications,” *Adv. Opt. Photonics* **3**, 161 (2011).
- [17] M. Krenn, M. Malik, M. Erhard, and A. Zeilinger, “Orbital angular momentum of photons and the entanglement of Laguerre–Gaussian modes,” *Philos. Trans. R. Soc. A* **375**, 20150442 (2017).
- [18] A. Mair, A. Vaziri, G. Weihs, and A. Zeilinger, “Entanglement of the orbital angular momentum states of photons,” *Nature* **412**, 313 (2001).
- [19] J. Leach, B. Jack, J. Romero, A. K. Jha, A. M. Yao, S. Franke-Arnold, D. G. Ireland, R. W. Boyd, S. M. Barnett, and M. J. Padgett, “Quantum correlations in optical angle–orbital angular momentum variables,” *Science* **329**, 662 (2010).
- [20] P. Carruthers and M. M. Nieto, “Phase and angle variables in quantum mechanics,” *Rev. Mod. Phys.* **40**, 411 (1968).
- [21] A. S. Holevo, *Probabilistic and Statistical Aspects of Quantum Theory*, 2nd ed., Publications of the Scuola Normale Superiore (Edizioni della Normale, Pisa, 2011).
- [22] K. Kowalski, J. Rembieliński, and L. Papaloucas, “Coherent states for a quantum particle on a circle,” *J. Phys. A: Math. Gen.* **29**, 4149 (1996).
- [23] H. A. Kastrup, “Wigner functions for the pair angle and orbital angular momentum,” *Phys. Rev. A* **94**, 062113 (2016).
- [24] Z. Hradil, J. Řeháček, Z. Bouchal, R. Čechovský, and L. Sánchez-Soto, “Minimum uncertainty measurements of angle and angular momentum,” *Phys. Rev. Lett.* **97**, 243601 (2006).
- [25] N. W. McLachlan, *Theory and Application of Mathieu Functions*, 1st ed. (Clarendon Press, Oxford, 1947).
- [26] S. Goldstein, “XVII.– On the asymptotic expansion of the characteristic numbers of the Mathieu equation,” *Proceedings of the Royal Society of Edinburgh* **49**, 210 (1930).
- [27] A. Lukš, V. Peřinová, and J. Křepelka, “Special states of the plane rotator relevant to the light field,” *Phys. Rev. A* **46**, 489 (1992).
- [28] Z. Hradil, J. Řeháček, A. B. Klimov, I. Rigas, and L. L. Sánchez-Soto, “Angular performance measure for tighter uncertainty relations,” *Phys. Rev. A* **81**, 014103 (2010).
- [29] T. Opatrný, “Mean value and uncertainty of optical phase—a simple mechanical analogy,” *J. Phys. A: Math. Gen.* **27**, 7201 (1994).
- [30] B.-G. Englert, “Uncertainty relations revisited,” *Phys. Lett. A* **494**, 129278 (2024).
- [31] H. F. Hofmann and S. Takeuchi, “Violation of local uncertainty relations as a signature of entanglement,” *Phys. Rev. A* **68**, 032103 (2003).
- [32] Z. Hradil, “Phase measurement in quantum optics,” *Quantum Opt.: J. Euro. Opt. Soc. B* **4**, 93 (1992).
- [33] M. Ban, “Relative number state representation and phase operator for physical systems,” *J. Math. Phys.* **32**, 3077 (1991).
- [34] Y. Makhlin, G. Schön, and A. Shnirman, “Quantum-state engineering with Josephson-junction devices,” *Rev. Mod. Phys.* **73**, 357 (2001).
- [35] M. H. Devoret, A. Wallraff, and J. M. Martinis, “Superconducting qubits: A short review,” arXiv:0411174.
- [36] S. Kwon, A. Tomonaga, G. Lakshmi Bhai, S. J. Devitt, and J.-S. Tsai, “Gate-based superconducting quantum computing,” *J. Appl. Phys.* **129**, 041102 (2021).
- [37] A. Blais, A. L. Grimsmo, S. M. Girvin, and A. Wallraff, “Circuit quantum electrodynamics,” *Rev. Mod. Phys.* **93**, 025005 (2021).

Appendix A: Derivation of moment of inertia for arbitrary axis

Here we give a simple and straightforward proof of the moment of inertia (28) without using tensor calculations. Assume the coordinate system of the unit ring, where X axis goes through its center of mass, vectors of axis of rotation $\mathbf{n} = (\cos \Phi \sin \theta, \sin \Phi \sin \theta, \cos \theta)$ and position on the unit ring at the $X - Y$ plane $\mathbf{e} = (\cos \varphi, \sin \varphi, 0)$. The moment of inertia of the ring with respect to the axis at origin is given as

$$M_0 = \langle \sin^2 \vartheta \rangle_\varphi, \quad (\text{A1})$$

where $\cos \vartheta = \mathbf{n} \cdot \mathbf{e} = \cos(\Phi - \varphi) \sin \theta$. The moment of inertia with respect to parallel axis in the center of mass is given by the parallel axis theorem as

$$M = M_0 - |\langle C \rangle|^2 \cos^2 \theta. \quad (\text{A2})$$

Using the relation $D^2 = 1 - |\langle C \rangle|^2$ and $D^2 = \langle [\Delta S(\Phi)]^2 \rangle + \langle [\Delta C(\Phi)]^2 \rangle$ we get finally the expression where the moment of inertia is given as weighted sum of both cosine and sine variances

$$M = D^2 - \langle [\Delta C(\Phi)]^2 \rangle \sin^2 \theta \quad (\text{A3})$$

$$= \langle [\Delta S(\Phi)]^2 \rangle + \langle [\Delta C(\Phi)]^2 \rangle \cos^2 \theta. \quad (\text{A4})$$

Appendix B: The tight uncertainty relations for generic moment of inertia

There are two ways motivated by previous approach. There are three parameters of the covariance matrix (13), e.g., its trace, determinant and relative phase between moments or just moments $\langle E \rangle, \langle E^2 \rangle$ (apart of an overall arbitrary phase) which can be exploited for quantification of the “noise” associated with the covariance matrix.

The first formulation is motivated by a similar approach as in (6) seeking the minimum of the variance of angular momentum under the constraint of fixed values of moments $\langle E \rangle$ and $\langle E^2 \rangle$

$$\langle (\Delta L)^2 \rangle \geq B(\langle E \rangle, \langle E^2 \rangle). \quad (\text{B1})$$

The extremal states and the uncertainty can be found as solution of the ground state of the Hamiltonian

$$\left(L^2 + \mu L + \frac{1}{2} q^* E + \frac{1}{2} q E^\dagger + \frac{1}{2} r^* E^2 + \frac{1}{2} r E^{2\dagger} \right) |\Psi\rangle = a |\Psi\rangle, \quad (\text{B2})$$

μ, q, r being Lagrange multipliers. Since we are seeking the solution for $\langle L \rangle = 0$ and zero phase, we might set $\mu = 0$ an in ϕ -representation this tends to Hill equation, similarly to previously discussed problem of Mathieu function,

$$-\psi''(\phi) + [q \cos(\phi) + r \cos(2\phi - \beta)] \psi(\phi) = a \psi(\phi), \quad (\text{B3})$$

$\beta = \arg[\langle E^2 \rangle \langle E \rangle^{*2}]$. Inequality (B1) should be further modified in a similar way as it was done in (17) in order to identify the angular uncertainty term.

The second formulation will require to minimize the product $\langle (\Delta L)^2 \rangle M_{\mathbf{n}}$ for fixed values of θ, Φ . This corresponds to fixed values D^2 and $\langle (\Delta C(\Phi))^2 \rangle$, it means just two constraints in Hill equation. Finally, the product should be minimised with respect to θ, Φ , which should be finally identified as state dependent quantities

$$\langle (\Delta L)^2 \rangle M_{\mathbf{n}} \geq C(\langle E \rangle, \langle E^2 \rangle). \quad (\text{B4})$$

Notice by passing that von Mises state - a solution of Eq. (12), can be cast as a special case of Hill equation corresponding to the ground state of the Hamiltonian

$$(\Delta L + i\kappa \Delta S_\alpha) |(\Delta L - i\kappa \Delta S_\alpha) |\psi\rangle = 0. \quad (\text{B5})$$

Appendix C: Saturable bounds for simultaneous measurement

In this section we analyse the inequalities for the uncertainty products

$$\Pi_{\mathcal{D}} = \langle (\Delta \mathcal{L})^2 \rangle \mathcal{D}^2, \quad (\text{C1})$$

$$\Pi_{\mathcal{S}} = \langle (\Delta \mathcal{L})^2 \rangle \langle (\Delta \mathcal{S})^2 \rangle, \quad (\text{C2})$$

where the uncertainties on the RHS are defined in Eqs. (33)-(35) of the main text. First, we analyse the product of uncertainties with dispersion and then move on to the case containing the variance of the sine operator.

1. Bounds for uncertainty product $\Pi_{\mathcal{D}}$

At the outset it is convenient to introduce the vectors

$$\boldsymbol{\ell}_{ij} = (\Delta L_i, \Delta L_j)^T, \quad \mathbf{d}_{ij} = (\langle E_i \rangle |D_j, D_i\rangle^T, \quad (\text{C3})$$

where $i, j = s, a$, and $\Delta A \equiv \sqrt{\langle (\Delta A)^2 \rangle}$. This allows us to write

$$\langle (\Delta \mathcal{L})^2 \rangle = \|\boldsymbol{\ell}_{sa}\|^2 = \|\boldsymbol{\ell}_{as}\|^2, \quad (\text{C4})$$

$$\mathcal{D}^2 = \|\mathbf{d}_{sa}\|^2 = \|\mathbf{d}_{as}\|^2, \quad (\text{C5})$$

and express the product (C1) in the following four different ways:

$$\Pi_{\mathcal{D}} = \|\boldsymbol{\ell}_{ij}\|^2 \|\mathbf{d}_{kl}\|^2, \quad (\text{C6})$$

where $(ij, kl) = (sa, sa), (sa, as), (as, sa), (as, as)$. Each combination leads to a different bound whereby the bounds corresponding to the combinations (as, sa) and (as, as) are not better than the other two bounds. If we restrict ourselves to cases corresponding to combinations (sa, sa) and (sa, as) and introduce for simplicity the denotation $\boldsymbol{\ell} \equiv \boldsymbol{\ell}_{sa}$ we get the following estimates

$$\begin{aligned} \Pi_{\mathcal{D}} &= \|\boldsymbol{\ell}\|^2 \|\mathbf{d}_{ij}\|^2 \geq |(\boldsymbol{\ell}^T \cdot \mathbf{d}_{ij})|^2 \\ &= \begin{cases} (\langle E_s \rangle |\Delta L_s D_a + \Delta L_a D_s|^2 \equiv \mathcal{A}_1 & \text{for } ij = sa; \\ (\langle E_a \rangle |\Delta L_s D_s + \Delta L_a D_a|^2 \\ \geq (\langle E_a \rangle |\sqrt{B_s} + \sqrt{B_a}|)^2 \equiv \mathcal{A}_2 & \text{for } ij = as. \end{cases} \quad (\text{C7}) \end{aligned}$$

The inequality 1 is a consequence of the Cauchy-Schwarz inequality and it is saturated for $\boldsymbol{\ell} = \lambda \mathbf{d}_{ij}$, i.e., for $ij = sa$ when

$$\Delta L_s D_s = \langle E_s \rangle |\Delta L_a D_a| \quad (\text{C8})$$

holds, whereas for $ij = as$ when

$$\Delta L_s D_a = \langle E_a \rangle |\Delta L_a D_s| \quad (\text{C9})$$

is satisfied. The inequality 2 then follows from uncertainty relations (6) of the main text for the signal and ancilla, where we used the abbreviation $B_s \equiv B(D_s), B_a \equiv B(D_a)$. This justifies the metrological role of extremal states since saturation is achieved for signal and ancilla prepared in Mathieu state with the uncertainties matching the condition (C9).

If we limit ourselves to cases where the ancilla is prepared in the Mathieu state $|ce_0, q_a\rangle_a$, we have $\Delta L_a D_a \leq 1/2$ (see red line in Fig. 3 of the main text), and the signal state then would have to satisfy $\Delta L_s D_s \leq \langle E_s \rangle / 2$. However, this would contradict to unsaturable inequality $\Delta L_s D_s \geq \langle E_s \rangle / 2$ following from inequality 4 of (17). Thus the condition (C8) can only be satisfied for $\langle E_s \rangle = 0$ implying $D_s^2 = 1$ and $\langle (\Delta L_s)^2 \rangle = 0$, and the optimal signal state is an angular momentum eigenstate $|l\rangle_s$. The branch \mathcal{A}_1 in Eq. (C7) then reduces to $\mathcal{A}_1 = \langle (\Delta L_a)^2 \rangle$ and it lies below the branch \mathcal{A}_2 of the same equation. The two branches intersect if $(\Delta L_a - \sqrt{B_a}) / \langle E_a \rangle = \sqrt{B_s}$, which happens for $q_{a,\text{int}} \doteq 9.29$ giving $D_{a,\text{int}}^2 \doteq 0.3$. For larger D_a the branch \mathcal{A}_2 is, on the other hand, less than the branch \mathcal{A}_1 . Thus assuming the ancilla prepared in the Mathieu state we find the uncertainty product $\Pi_{\mathcal{D}}$, Eq. (C7), to be bounded from below by

$$\mathcal{B}_{\mathcal{D}} = \begin{cases} (\langle E_a \rangle |\sqrt{B_s} + \sqrt{B_a}|)^2 & \text{for } D_{a,\text{int}}^2 > D_a^2 \geq 0; \\ \langle (\Delta L_a)^2 \rangle & \text{for } 1 \geq D_a^2 \geq D_{a,\text{int}}^2. \end{cases} \quad (\text{C10})$$

It is of interest to compare the obtained bounds with the minimum of the uncertainty product (C1) for the Mathieu states $|ce_0, q_s\rangle_s |ce_0, q_a\rangle_a$. Numerical minimization of the product over q_s at fixed q_a yields on a restricted interval of dispersions D_a^2 a little lower bound compared to the bound (C10). The resulting function is depicted by a solid black line in Fig. 3 of the main text. Similar to the bound (C10) the obtained curve again contains a sharp point, but now for a slightly different $q_{a,\text{sh}} \doteq 8.7$, for which $D_{a,\text{sh}}^2 \doteq 0.31$. In the

region $1 \geq D_a^2 \geq D_{a,\text{sh}}^2$ the obtained numerical curve coincides exactly with the second branch $\langle(\Delta L_a)^2\rangle$ of the bound (C10), whereas for $D_{a,\text{sh}}^2 > D_a^2 \geq 0$ the numerically found minimal uncertainty product lies a little below the first branch $(\langle E_a \rangle \sqrt{B_s} + \sqrt{B_a})^2$ (c.f. solid black line and solid magenta line in white area of Fig. 3). For comparison, in Fig. 3 we also plotted by the dashed orange line the minimal uncertainty product for the product $|0, 0, \kappa_s\rangle_s |0, 0, \kappa_a\rangle_a$ of the von Mises states and by the dashed green line the uncertainty product for von Mises states satisfying the condition (C9). We see that in both cases the obtain curves are again only a little worse than the black and magenta line for the Mathieu states. The observed subtle differences between separate solutions as well as Mathieu and von Mises states will become important when the experimental techniques will be able to distinguish among them.

2. Bounds for uncertainty product $\Pi_{\mathcal{S}}$

Moving to the uncertainty product (C2), assume for simplicity the signal and ancilla to be prepared in the von Mises states $|n, \alpha, \kappa_s\rangle_s$ and $|0, 0, \kappa_a\rangle_a$, respectively. Let us further introduce the vector

$$\mathbf{s}_{ij} = \left(\sqrt{\langle E_i^2 \rangle} |\Delta S_j, \Delta S_i \rangle^T, \quad (\text{C11})$$

where

$$\begin{aligned} \Delta S_j &= \sqrt{\langle (\Delta S_j)^2 \rangle} = \sqrt{\langle S_{j, \arg(E_j)}^2 \rangle} \\ &= \sqrt{\frac{1}{2} (1 - \langle E_j^2 \rangle)}. \end{aligned} \quad (\text{C12})$$

Similar to Eqs. (C5) and (C6) we can then write

$$\langle (\Delta \mathcal{S})^2 \rangle = \|\mathbf{s}_{sa}\|^2 = \|\mathbf{s}_{as}\|^2, \quad (\text{C13})$$

and

$$\Pi_{\mathcal{S}} = \|\boldsymbol{\ell}\|^2 \|\mathbf{s}_{kl}\|^2, \quad (\text{C14})$$

where $(ij, kl) = (sa, sa), (sa, as), (as, sa), (as, as)$. Again, there are four ways of how we can decompose the uncertainty product (C2) but only combinations (sa, sa) and (sa, as) are relevant. Consequently, we get for the uncertainty product (C2) the following inequalities

$$\begin{aligned} \Pi_{\mathcal{S}} &= \|\boldsymbol{\ell}\|^2 \|\mathbf{s}_{ij}\|^2 \geq |(\boldsymbol{\ell}^T \cdot \mathbf{s}_{ij})|^2 \\ &= \begin{cases} \left(\sqrt{\langle E_s^2 \rangle} |\Delta L_s \Delta S_a + \Delta L_a \Delta S_s| \right)^2 \equiv \mathcal{C}_1 & \text{for } ij = sa; \\ \left(\sqrt{\langle E_a^2 \rangle} |\Delta L_s \Delta S_s + \Delta L_a \Delta S_a| \right)^2 \\ \geq \frac{1}{4} \left(\sqrt{\langle E_a^2 \rangle} |\langle E_s \rangle| + |\langle E_a \rangle| \right)^2 \equiv \mathcal{C}_2 & \text{for } ij = as. \end{cases} \end{aligned} \quad (\text{C15})$$

Here, to get inequality 1 we used the Cauchy-Schwarz inequality and the equality is obtained if and only if $\boldsymbol{\ell} = \lambda \mathbf{s}_{ij}$, i.e., for $ij = sa$ when

$$\Delta L_s \Delta S_s = \sqrt{\langle E_s^2 \rangle} |\Delta L_a \Delta S_a| \quad (\text{C16})$$

is obeyed, whereas for $ij = as$ when

$$\Delta L_s \Delta S_a = \sqrt{\langle E_a^2 \rangle} |\Delta L_a \Delta S_s| \quad (\text{C17})$$

is fulfilled. The inequality 2 then comes from the uncertainty relation [11]

$$\langle (\Delta L_j)^2 \rangle \langle (\Delta S_j)^2 \rangle \geq \frac{1}{4} |\langle E_j \rangle|^2, \quad (\text{C18})$$

where $j = s, a$. Substituting here from [11]

$$\langle (\Delta L_j)^2 \rangle = \frac{\kappa_j I_1(2\kappa_j)}{2 I_0(2\kappa_j)}, \quad \langle (\Delta S_j)^2 \rangle = \frac{1}{2\kappa_j} \frac{I_1(2\kappa_j)}{I_0(2\kappa_j)}, \quad (\text{C19})$$

we find that in terms of the parameters κ_s and κ_a the condition (C16) reads as

$$\frac{I_1(2\kappa_s)}{I_0(2\kappa_s)} = \sqrt{\frac{I_2(2\kappa_s) I_1(2\kappa_a)}{I_0(2\kappa_s) I_0(2\kappa_a)}}. \quad (\text{C20})$$

Likewise, the condition (C17) boils down to [11]

$$\kappa_s = \sqrt{\frac{I_2(2\kappa_a)}{I_0(2\kappa_a)}}^{\kappa_a}. \quad (\text{C21})$$

Numerical analysis reveals that for a given κ_a the condition (C20) is satisfied by $\kappa_s = 0$. This gives $\langle (\Delta L_s)^2 \rangle = 0$ and it is again optimal to measure the angular momentum eigenstates $|l\rangle_s$. What is more, $\langle (\Delta S_s)^2 \rangle = 1/2$ and the branch \mathcal{C}_1 reduces to $\mathcal{C}_1 = \langle (\Delta L_a)^2 \rangle / 2$. The latter branch intersects with the second branch \mathcal{C}_2 , Eq. (C15), for κ_a satisfying the following equation

$$\frac{\sqrt{2} \Delta L_a - |\langle E_a \rangle|}{\sqrt{\langle E_a^2 \rangle}} = |\langle E_s \rangle|, \quad (\text{C22})$$

where the parameter κ_s is given by the RHS of the condition (C21). Upon solving previous equation we find that the branches \mathcal{C}_1 and \mathcal{C}_2 intersect for $\kappa_{a,\text{int}} \doteq 3.018$ which gives $\tilde{D}_{a,\text{int}}^2 \doteq 0.167$. Since for $D_a^2 < \tilde{D}_{a,\text{int}}^2$ the branch \mathcal{C}_2 lies below the branch \mathcal{C}_1 , whereas for $D_a^2 > \tilde{D}_{a,\text{int}}^2$ it is the other way around, we find the uncertainty product (C2) to be greater or equal to

$$\mathcal{B}_{\mathcal{S}} = \begin{cases} \frac{1}{4} \left(\sqrt{\langle E_a^2 \rangle} |\langle E_s \rangle| + |\langle E_a \rangle| \right)^2 & \text{for } \tilde{D}_{a,\text{int}}^2 > D_a^2 \geq 0; \\ \frac{\langle (\Delta L_a)^2 \rangle}{2} & \text{for } 1 \geq D_a^2 \geq \tilde{D}_{a,\text{int}}^2. \end{cases} \quad (\text{C23})$$

The function (C23) is depicted by the red line in the inset of Fig. 4 of the main text. Its first branch is displayed by the magenta line in the main figure, as well as in the inset, where it consists of the dashed black line in the gray area and the solid red line in the white area. The second branch of the bound (C23) is depicted only in the inset and it consists of the solid red line in the gray area and solid black line in the white area. The value of the dispersion where the function (C23) exhibits the sharp point is $\tilde{D}_{a,\text{int}}^2 \doteq 0.167$ and it is depicted by the vertical border between the white and gray area.

By the numerical minimization of the uncertainty product (C2) over the parameter κ_s at fixed κ_a we get the black line in Fig. 4 of the main text. The line again possesses a sharp point but now for a slightly different value of $\kappa_{a,\text{sh}} \doteq 2.897$, for which $\tilde{D}_{a,\text{sh}}^2 \doteq 0.174$. Comparison with the numerically

minimized uncertainty product (C2) reveals that in the interval $1 \geq D_a^2 \geq \tilde{D}_{a,\text{sh}}^2$ the second branch $\langle(\Delta L_a)^2\rangle/2$ is equal to the minimal uncertainty product, whereas for $\tilde{D}_{a,\text{sh}}^2 > D_a^2 \geq 0$ the first branch lies slightly above the minimal uncertainty product (c.f. black line and magenta line in Fig. 4 of the main text).